

# Quantum network of superconducting qubits through opto-mechanical interface

Zhang-qi Yin<sup>1</sup>, W. L. Yang<sup>2</sup>, L. Sun<sup>1</sup>, L. M. Duan<sup>3,1</sup>

<sup>1</sup>Center for Quantum Information, IIS, Tsinghua University, Beijing 100084, P. R. China

<sup>2</sup>State Key Laboratory of Magnetic Resonance and Atomic and Molecular Physics, Wuhan Institute of Physics and Mathematics, Chinese Academy of Sciences, Wuhan 430071, China and

<sup>3</sup>Department of Physics, University of Michigan, Ann Arbor, Michigan 48109, USA

(Dated: July 17, 2018)

We propose a scheme to realize quantum networking of superconducting qubits based on the opto-mechanical interface. The superconducting qubits interact with the microwave photons, which then couple to the optical photons through the opto-mechanical interface. The interface generates a quantum link between superconducting qubits and optical flying qubits with tunable pulse shapes and carrier frequencies, enabling transmission of quantum information to other superconducting or atomic qubits. We show that the scheme works under realistic experimental conditions and it also provides a way for fast initialization of the superconducting qubits under 1 K instead of 20 mK operation temperature.

## I. INTRODUCTION

Superconducting qubits (SQs) constitute one of the leading candidate systems for realization of quantum computation [1]. Through the circuit resonators, SQs have strong coupling to the microwave photons [1], which can be used for qubit interaction, state engineering of the photonic modes, and non-destructive readout of the qubits [2, 3]. Universal quantum logic gates have been realized for SQs in circuit QED (cQED) systems with high fidelity and speed [4]. Through use of the noise insensitive qubits, the coherent time of the SQs has been increased by several orders of magnitude in recent years and pushed to the 100  $\mu$ s region [5, 6]. In a single circuit resonator, the number of SQs is still limited. Further scaling up the number of qubits requires linking distant cQED systems to form a quantum network. Microwave photons are sensitive to thermal noise and their quantum states only survive under cryogenic temperature. So it is hard to use them to link SQs in two different setups. Optical photons, on the other hand, are robust information carriers at room temperature and serve as ideal flying qubits for long-distance communication. They can carry quantum information to distant locations through an optical fiber.

In this paper, we propose a scheme to realize a quantum network of SQs through an opto-mechanical interface that couples optical photons in a cavity to microwave photons and SQs in a circuit resonator. The interface generates entangled states between SQs and photonic pulses with tunable pulse shape and carrier frequency. The photons then make a quantum link between distant SQs through either a measurement-based entangling protocol or a deterministic state mapping. Because of the tunability of shape and frequency of the emitted photon, the same scheme can also be used to realize a hybrid network between SQs and other matter qubits such as atomic ions [7], quantum dots [8], or defect spins in solids [9]. A hybrid network may allow combination of advantages of different kinds of qubits. For instance, SQs may be good for fast information processing while atomic qubits are ideal for quantum memory. Our scheme is based on the recent advance on the microwave-optical interface: there have been several proposals to realize this interface with ions [10, 11], cold atoms [12], or a hybrid opto-mechanical system with superconducting res-

onators [13–19], or with flux qubit [20]. In particular, a recent experiment has demonstrated the transducer between microwave and optical photons using the opto-mechanical system at 4.5K temperature [21]. One hassle for an interface between SQs and optical photons is that thermal initialization of the SQs requires an operating temperature around 20 mK in a dilution fridge, while an interface to photons requires an optical window, which introduces heating due to black-body radiation and may significantly increase the system temperature. We circumvent this problem by showing that our proposed scheme can achieve fast initialization of the SQs at 1 K through optical sideband cooling by use of the same opto-mechanical interface.

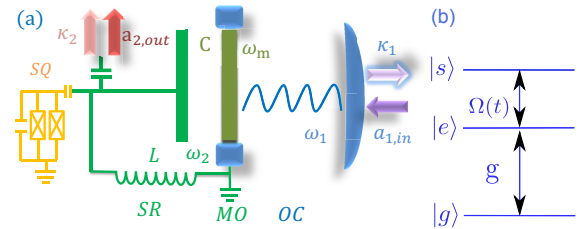


FIG. 1: (Color online) (a) The schematic scheme of the opto-mechanical quantum interface. The SQ couples with the microwave mode  $a_2$  in a superconducting resonator (SR). The mechanical oscillator (MO) mode  $a_m$  for vibration of the interface couples simultaneously to the mode  $a_2$  of the SR and the mode  $a_1$  of the optical cavity (OC). Both  $a_2$  and  $a_1$  modes are driven by coherent classical fields on the red sideband. (b) The energy levels of the superconducting junction, where  $|g\rangle$  is the ground state,  $|e\rangle$  is the first excited state, and  $|s\rangle$  is the second excited state. The transition  $|g\rangle$  to  $|e\rangle$  couples to the mode  $a_2$  with coupling rate  $g_c$ , while transition  $|e\rangle$  to  $|s\rangle$  is driven by a microwave field with Rabi frequency  $\Omega(t)$ .

## II. THE MODEL

As show in Fig. 1, the system we consider contains an optical cavity (OC) and a microwave superconducting resonator (SR) [22, 23], which share an interface that can vibrate and forms a mechanical oscillator (MO) [24, 25]. The shared vi-

brating interface between the OC and the SR has been proposed in several schemes [13–17] and realized very recently in experiments [21, 26]. For this system, the MO mode  $a_m$  of frequency  $\omega_m$  couples simultaneously to the optical mode  $a_1$  of frequency  $\omega_1$  and the microwave mode  $a_2$  of frequency  $\omega_2$ . We have assumed that the coupling rate is much less than the mode spacing of either of these oscillators so that only one mode is relevant respectively for the OC, the MO, and the SR. The optical and the microwave modes  $a_1$  and  $a_2$  are driven at the red-sideband with frequency  $\omega_{L1} = \omega_1 - \Delta_1$  and  $\omega_{L2} = \omega_2 - \Delta_2$ , respectively. We set  $\Delta_1 = \Delta_2 = \omega_m$ . Inside the SR, there are nonlinear Josephson junctions, with the lowest three anharmonic levels shown in Fig. 1b. The levels  $|g\rangle$  and  $|s\rangle$  make a SQ, with coupling mediated by the middle level  $|e\rangle$  with a coupling rate  $g_c$  for the  $|g\rangle \rightarrow |e\rangle$  transition and a Rabi frequency  $\Omega(t)$  (driven by a microwave field with tunable shape) for the  $|e\rangle \rightarrow |s\rangle$  transition.

The Hamiltonian of the system has the form  $H = H_0 + H_I + H_d$ , where  $H_0 = \sum_{i=1,2} \omega_i a_i^\dagger a_i + \omega_m a_m^\dagger a_m + \omega_e \sigma_{ee}$ ,  $H_I = \sum_{i=1,2} g_i a_i^\dagger a_i (a_m + a_m^\dagger) + g_c (\sigma_{eg} + \sigma_{ge}) (a_2 + a_2^\dagger)$ , and  $H_d = \sum_{i=1,2} (\frac{\Omega_i}{2} e^{-i\omega_{Li}t} + \text{h.c.}) (a_i + a_i^\dagger) + (\frac{\Omega'}{2} e^{-i\omega_{L2}t} + \text{h.c.}) (\sigma_{ge} + \sigma_{eg})$ . We have set  $\hbar = 1$  and taken the notation  $\sigma_{\mu\nu} = |\mu\rangle\langle\nu|$  ( $\mu, \nu = g, e, s$ ). The SQ and SR drive pulses are generated by two phase-locked microwave generators. The flux control pulses are used to tune the SQ to be resonant with the SR with  $\omega_2 = \omega_e$  [23]. The opto-mechanical coupling rates  $g_i$  ( $i = 1, 2$ ) are typically small, but their effect can be enhanced through the driving field  $\Omega_i$ . Under the driving, the steady state amplitude of the mode  $a_i$  is given by  $\alpha_i \approx \Omega_i / 2\Delta_i$ . We take the driving strength  $\Omega'^* = g_c \Omega_2 / \omega_m$ . The opto-mechanical coupling terms can be expanded with  $a_i - \alpha_i$  and the effective coupling Hamiltonian takes the form (see details in Appendix A) [15, 16, 27]

$$H_{om} = \sum_{i=1,2} \left[ \omega_m a_i^\dagger a_i + G_i (a_i^\dagger + a_i) (a_m + a_m^\dagger) \right] + \omega_m a_m^\dagger a_m + (g_c a_2 \sigma_{eg} + \text{h.c.}) \quad (1)$$

where  $G_i = \alpha_i g_i$ . Under the rotating wave approximation ( $\omega_m \gg G_i, g_c$ ), the whole Hamiltonian in the interaction picture is given by

$$H_I = (G_1 a_1^\dagger + G_2 a_2^\dagger) a_m + g_c \sigma_{eg} a_2 + \text{h.c.} \quad (2)$$

The corresponding Langevin equations for the  $a_j$  ( $j = 1, 2, m$ ) modes and the SQ take the form

$$\begin{aligned} \dot{a}_j &= -i[a_j, H_I] - \frac{\kappa_j}{2} + \sqrt{\kappa_j} a_j^{\text{in}}, \\ \dot{\sigma}_{ge} &= -i[\sigma_{ge}, H_I], -\frac{\gamma}{2} \sigma_{ge} + \sqrt{\gamma} \sigma_z a_s^{\text{in}}, \end{aligned} \quad (3)$$

where  $\sigma_z = \sigma_{ee} - \sigma_{gg}$ ,  $\gamma$  is the decay rate of the level  $|e\rangle$ , and  $\kappa_j$  is the decay rate of the mode  $a_j$ .

### III. SQ INITIALIZATION AND SQ-PHOTON QUANTUM INTERFACE

Without loss of generality, we take  $G_1 = G_2 = G$  for simplicity of notation. We may define the normal modes  $b, b_\pm$

with  $a_1 = (b_+ + b_- - \sqrt{2}b)/2$ ,  $a_2 = (b_+ + b_- + \sqrt{2}b)/2$ ,  $a_m = (b_+ - b_-)/\sqrt{2}$ , which diagonalize the opto-mechanical coupling Hamiltonian [28]. The SQ only resonantly couples with normal mode  $b$ . The normal mode  $b$  decays through two channels,  $a_1^{\text{out}}$  and  $a_2^{\text{out}}$ . The decay of  $b$  mode is denoted as  $\kappa = (\kappa_1 + \kappa_2)/2$ . Typically, we have  $\kappa_1 \gg \kappa_2$ , so the photons go out dominantly through the  $a_1^{\text{out}}$  channel, which is vacuum. As the SQ only strongly couples with the normal mode  $b$ , the steady state of SQ will approach to the ground state  $|g\rangle$ . If the SQ is initially in a mixture of  $|g\rangle$  and  $|e\rangle$  states, we can cool it to the ground state  $|g\rangle$  by driving the red sideband of the optical cavity [29–33]. If the initial state of the SQ involves mixture of other states, these other states can be first driven to the state  $|e\rangle$  through a microwave field and then decay to the ground state  $|g\rangle$  by the opto-mechanical sideband cooling. The working temperature for both initialization and interface can be much higher than tens of mK.

In order to couple the SQ to an output optical photon with controllable pulse shape, we prepare the SQ initially on the level  $|s\rangle$  and drive the transition  $|s\rangle$  to  $|e\rangle$  by a microwave field with Rabi frequency  $\Omega(t)$  and pulse duration  $T_D$ . The total Hamiltonian of the system is  $H_t = H_I + (\Omega(t)\sigma_{se} + \text{h.c.})$ . In the limit  $T_D^{-1} \ll G, g, \kappa_1$ , the modes  $b_\pm$  are not populated and can be adiabatically eliminated. The effective Hamiltonian is simplified to  $H_t = \Omega(t)\sigma_{se} + \frac{\sqrt{2}}{2} g_c b \sigma_{eg} + \text{h.c.}$  The Hamiltonian  $H_t$  has a dark state  $|D\rangle = [|s\rangle|0\rangle - r(t)|g\rangle|1\rangle] / \sqrt{1 + |r(t)|^2}$ , where  $r(t) = \sqrt{2}\Omega(t)/g_c$ , and  $|0\rangle, |1\rangle$  represent the Fock states of the mode  $b$ . To solve the output pulse shape, we rewrite the dark state as  $|D\rangle = \cos\theta|s\rangle|0\rangle - \sin\theta|g\rangle|1\rangle$ , with  $\cos\theta = 1/\sqrt{1 + |r|^2}$ , and define an orthogonal bright state  $|B\rangle = \sin\theta|s\rangle|0\rangle + \cos\theta|g\rangle|1\rangle$ . The wave-function of the whole system can be expanded as  $|\Psi\rangle = (c_d|D\rangle + c_b|B\rangle + c_e|e\rangle) \otimes |\text{vac}\rangle + |g\rangle|0\rangle \otimes |\varphi\rangle$ , where  $|\text{vac}\rangle$  is the vacuum state of output field, and  $|\varphi\rangle = \int_{-\omega_c}^{+\omega_c} d\omega c_\omega a_{out}^\dagger(\omega) |\text{vac}\rangle$  denotes the single-photon state of the output field with frequency spectrum  $c_\omega$ . The dynamics of system is determined by the Schrödinger equation  $i\partial_t |\Psi\rangle = H_t |\Psi\rangle$ , where  $H_t$  is the total Hamiltonian that includes the input-output coupling terms [34]. Using the method in Ref. [34], the output pulse shape  $f(t)$ , given by the Fourier transform of  $c_\omega$ , can be solved analytically in the adiabatic limit, with

$$f(t) = \sqrt{\kappa} \sin\theta \exp\left(-\frac{\kappa}{2} \int_0^t \sin^2\theta(\tau) d\tau\right). \quad (4)$$

The pulse shape  $f(t)$  is fully determined by  $\theta(t)$ .

To check whether the pulse shape of Eq. (4) derived under the adiabatic limit holds under typical experimental parameters, we compare in Fig. (2) the pulse shapes obtained from the analytic formula and from the exact numerical simulation. In numerical simulation, we solve the exact system dynamics by including the contribution of populations either in the bright state  $|B\rangle$  or of all the three modes  $b$  and  $b_\pm$ . As one can see from Fig. 2, if the pulse duration  $T_D \gtrsim 20/\kappa$ , the pulse shape from the analytic formula (4) overlaps very well with the exact result, with the mismatching error less than 1%. However, for a short pulse with  $T_D \sim 5/\kappa$ , there is a signifi-

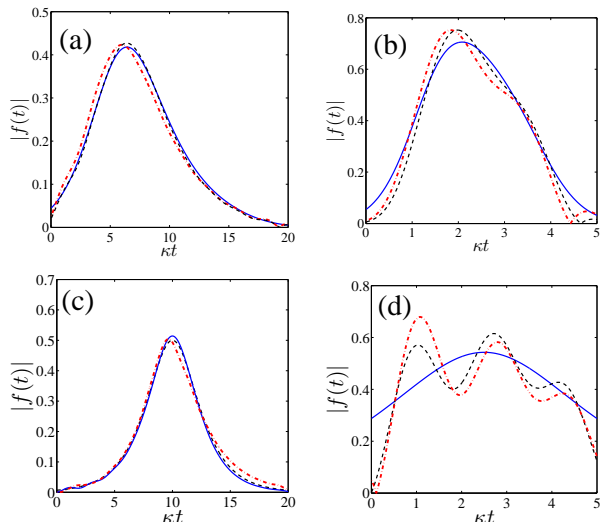


FIG. 2: (Color online) (a) The shape of the output single-photon pulse  $|f(t)|$ . We take  $g = G = 3\kappa$  and the pulse duration  $T_D = 20/\kappa$ . The driving pulses  $\Omega(t) = g e^{-(t-T_D/2)^2/2t_w^2}$  is assumed to be a Gaussian shape with the peak at  $t = T_D/2$  and a width  $t_w = T_D/5$ . The solid (dash, dash-dot) curve represents respectively the analytic pulse shape in Eq. (4) derived in the adiabatic limit (the numerical result that includes contribution of the bright state  $|B\rangle$ ), the exact result that includes contributions of all the modes  $b, b_\pm$ ). The shape function is normalized according to  $\int |f(t)|^2 dt = 1$  for the convenience of comparison. The overlap between the exact shape (dash-dot curve) and the adiabatic shape (solid curve) is about 99%. (b) Same as Fig. (a) but with the pulse duration  $T_D = 5/\kappa$ . The adiabatic approximation is not well satisfied in this case, and the shape overlap is reduced to 80%. (c) Same as Fig. (a) but with the driving Rabi frequency  $\Omega(t) = (g_c/\sqrt{2}) e^{\kappa(t-T_D/2)/2}$ , which gives a symmetric output pulse shape [34]. In the adiabatic limit, the shape (the solid curve) is given by the analytic form  $f(t) = \sqrt{\kappa/4} \text{sech}[\kappa(t-T_D/2)/2]$ , which has overlap of 99.7% with the exact shape. (d) Same as Fig. (c) but with the pulse duration  $T_D = 5/\kappa$ .

cant shape mismatching error and one should use the exact result instead of the approximate analytic formula. The exact result shows some oscillations in the pulse shape for a short driving field, resulting from the population oscillation in different modes  $b, b_\pm$  when the condition of adiabatic elimination  $T_D^{-1} \ll G, g, \kappa_1$  is not well satisfied.

#### IV. QUANTUM NETWORKING OF SQS

In the above, we have shown how to couple a SQ to a single optical output photon with a controllable pulse shape. This ability is critical for building up a quantum network of SQs or a hybrid network between SQs and other matter qubits. Here, we mention two complementary schemes for quantum networking of SQs, requiring different kinds of pulse shape control.

The key requirement of quantum networking is to generate entanglement between remote SQs. The first scheme for entanglement generation is based on a deterministic quantum

state transfer between SQs in two remote cavities [35]. As absorption is the time reversal of the emission process, it has been shown in Ref. [35] that an emitted single-photon pulse can be completely absorbed by a matter qubit in a cavity if we simultaneously reverse the temporal shape of the photon pulse and the driving field  $\Omega(t)$ . As shown in Fig. 2, with an appropriate control of the driving microwave field  $\Omega(t)$ , we can transfer a quantum state from a SQ to a single-photon pulse with a symmetric temporal shape. This single-photon pulse, after propagation in an optical fiber, can then be absorbed by a SQ in another remote cavity, if the driving  $\Omega'(t)$  of the second SQ is the time reversal of  $\Omega(t)$ . The shape control of the driving microwave pulse  $\Omega(t)$  or  $\Omega'(t)$  can be easily achieved through modulation by an arbitrary wave form generator. If we make a half transfer of the population from the first SQ to the photonic pulse, the generated state between the SQ and the output photon  $p$  has the form  $(|s\rangle_1|0\rangle_p + |g\rangle_1|1\rangle_p)/\sqrt{2}$ . Then, after absorption of the photon by the second SQ, we generate an entangled state  $(|s\rangle_1|g\rangle_2 + |g\rangle_1|s\rangle_2)/\sqrt{2}$  between two remote SQs, as required for quantum networking.

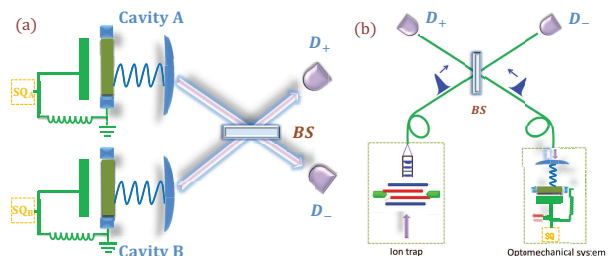


FIG. 3: (Color online) (a) The schematic to generate entanglement between remote SQs. Two SQs are located in distant cavities A and B. The SQs with dashed boxes represent the same structure as the orange part (SQ) in Fig. 1a, capacitively coupled to the SRs. The SQs couple to the output photons through opto-mechanical interfaces. The output photons, after propagation, interfere at a beam splitter and then are detected by single-photon counters. Registration of a photon-count generates entanglement between the remote SQs. (b) The same setup can be used to entangle SQs with other kinds of matter qubits, such as trapped ions. The carrier frequency and shape of the photon from the SQ is tuned by the opto-mechanical interface to match with the photon pulse from other matter qubits.

The entanglement between remote SQs can also be generated in a probabilistic fashion through detection of interference of the emitted photon(s) [34, 36, 37]. For instance, as shown in Fig. 4a, we have SQs in two remote cavities, each emitting a single-photon pulse with a small probability  $p_0 = 1 - \exp[-\kappa \int_0^{T_D} \sin^2 \theta(\tau) d\tau]$  through an incomplete adiabatic passage from the state  $|s\rangle$  to  $|g\rangle$ . The emitted pulses, after propagation in optical channels, interfere at a 50 – 50% beam splitter, with outputs detected by single-photon counters. If we register only one photon from these detectors, the two SQs are projected to an entangled state  $(|s\rangle_1|g\rangle_2 + e^{i\varphi}|g\rangle_1|s\rangle_2)/\sqrt{2}$  with a success probability proportional to  $p_0 \ll 1$ . The unknown relative phase  $\varphi$  can be canceled during the detection process [38], or through the second round of entanglement generation by applying the same protocol again [39]. Com-

pared with the deterministic scheme [35], this probabilistic scheme has a lower efficiency as the protocol needs to be repeated until one successfully registers a photon count, however, it is more robust to noise as the photon loss in the optical channels does not influence the fidelity of this scheme.

A major challenge for quantum networking based on the photonic connection is to achieve the spectrum (shape) and frequency matching of the emitted photon pulses from different matter qubits. For solid-state qubits in particular, the coupling parameters usually vary for different systems and it is hard to get identical qubits or coupling rates. A remarkable advantage of the scheme based on the opto-mechanical interface is that all the mismatches in frequencies or pulse shapes can be easily compensated through the driving fields. For instance, the scheme works perfectly well if the coupling or decay rates are different for different systems. As the pulse shape only depends on  $\theta(t)$  from Eq. (4), we can always get identical shapes as difference in the coupling rates can be easily compensated by the microwave driving amplitude  $\Omega(t)$ . Furthermore, the output optical frequency is purely determined by the eigenmode structure of the optical cavity and not limited by the qubit parameters. So, depending on the frequency and shape of the driving field, we can have a quantum interface between the SQ and the optical photon with widely tunable carrier frequency and shape, which can then interfere with the photons emitted by other kinds of matter qubits, such as trapped ions [40], quantum dots [8, 41], or diamond nitrogen vacancy centers [9]. The SQ-opto-mechanical interface therefore can work as a quantum transducer to generate entanglement links between different types of matter qubits. This leads to a hybrid quantum network, with an example illustrated in Fig. 3(b), which has the important advantage to combine the particular strength of each kind of matter qubits.

## V. SQ INITIALIZATION FIDELITY AND INTERFACE EFFICIENCY

In the above analysis, we assume the SQ couples dominantly to the output field of the optical cavity and neglect other dissipation channels. Now we take into account all the other dissipation processes and calculate their effects on the fidelity of quantum interface. Under the condition that the pulse duration  $T_D^{-1} \ll G, g, \kappa_1$ , we can adiabatically eliminate all the modes  $a_j$  ( $j = 1, 2, m$ ) in the Langevin equations (3) and arrive at the following decay equation for the SQ (see details in Appendix B):

$$\dot{\sigma}_{ge} = -\frac{\gamma_{eff}}{2}\sigma_{ge} + \sqrt{\gamma_{eff}}\sigma_z a_{eff}^{in}, \quad (5)$$

where  $\gamma_{eff} = \gamma + \tilde{\kappa}_1 + \tilde{\kappa}_2 + \tilde{\kappa}_m$ ,  $a_{eff}^{in} = [-i\sqrt{\tilde{\kappa}_1}a_1^{in} + i\sqrt{\tilde{\kappa}_2}a_2^{in} + \sqrt{\gamma}a_s^{in} + \sqrt{\tilde{\kappa}_m}a_m^{in}]/\sqrt{\gamma_{eff}}$ ,  $\tilde{\kappa}_1 = \frac{4g^2\kappa_1}{(\kappa_1+\kappa_2+\kappa_1\kappa_2\kappa_m/4G^2)^2}$ ,  $\tilde{\kappa}_2 = \frac{(2+\kappa_1\kappa_m/2G^2)^2g^2\kappa_2}{(\kappa_1+\kappa_2+\kappa_1\kappa_2\kappa_m/4G^2)^2}$ , and  $\tilde{\kappa}_m = \frac{g^2\kappa_m^2/G^2}{(\kappa_1+\kappa_2+\kappa_1\kappa_2\kappa_m/4G^2)^2}$ . The physical meaning of Eq. (5) is clear: the SQ couples to four decay channels, the optical channel  $a_1^{in}$  with decay rate  $\tilde{\kappa}_1$ , the microwave channel  $a_2^{in}$  with decay rate  $\tilde{\kappa}_2$ , the mechanical channel  $a_m^{in}$  with decay rate  $\tilde{\kappa}_m$ , and the intrinsic channel  $a_s^{in}$  with

decay rate  $\gamma$ . For each decay channel, the effective dissipation rate is given by  $(\bar{n}_j + 1)\tilde{\kappa}_j$ , where  $\bar{n}_j = 1/(\exp(\hbar\omega_j/k_B T) - 1)$  is the mean thermal photon (or phonon) number and  $T$  denotes temperature of the system. The initialization of the SQ is described by the Langevin equation (5) and the final probability  $P_g$  for the SQ in the state  $|g\rangle$  is determined by the stationary state under Eq. (5) (after a decay time of the order of  $1/\tilde{\kappa}_1 \sim 10$  ns with

$$P_g = \frac{\tilde{\kappa}_1 + (n_2 + 1)\tilde{\kappa}_2 + (n_m + 1)\tilde{\kappa}_m}{\tilde{\kappa}_1 + (2n_2 + 1)(\gamma + \tilde{\kappa}_2) + (2n_m + 1)\tilde{\kappa}_m}. \quad (6)$$

Under experimental parameters list in the caption of Fig. (4) and 1 K system temperature, the fidelity  $P_g$  for state initialization is larger than 99% (we assume temperature  $T = 1$  K with  $\bar{n}_2 = 1.62$ , and  $\bar{n}_m = 2.08 \times 10^3$ ).

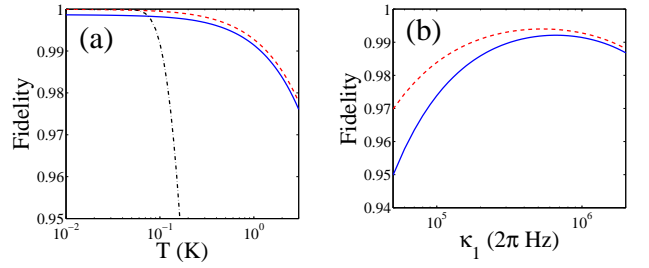


FIG. 4: (Color online) (a) The temperature dependence of the fidelity  $F$  (solid curve) of quantum interface and the fidelity  $P_g$  (dashed curve) for state initialization. The dash-dotted curve shows the probability in the ground state without opto-mechanical sideband cooling. The parameters are taken as  $\omega_1/2\pi = 200$  THz,  $\omega_2/2\pi = 10$  GHz, and  $\omega_m/2\pi = 10$  MHz [24, 25, 42],  $\kappa_1/2\pi = 10$  MHz,  $\kappa_2/2\pi = 1$  kHz,  $\kappa_m/2\pi = 10$  Hz [43],  $\gamma/2\pi = 5$  kHz [44, 45],  $G/2\pi = 1$  MHz, and  $g_c/2\pi = 1$  MHz. (b) The dependence of the fidelity  $F$  (solid curve) and  $P_g$  (dashed curve) on the optical cavity decay rate  $\kappa_1$  at 1 K temperature. The other parameters are the same as Fig. (a).

For quantum networking of SQs through the optical decay channel, all the other dissipation channels contribute to noise, and the fidelity  $F$  of the quantum interface can be estimated by the relative ratio of the optical decay rate to the total dissipation rate

$$F = \frac{\tilde{\kappa}_1}{\tilde{\kappa}_1 + (\bar{n}_2 + 1)\tilde{\kappa}_2 + (\bar{n}_m + 1)\tilde{\kappa}_m + (\bar{n}_2 + 1)\gamma}, \quad (7)$$

where we have taken  $\bar{n}_1 \approx 0$  at the optical frequency. The experimental parameters typically satisfy  $G \sim \kappa_1 \gg \kappa_2, \kappa_m, \gamma$ . In this case,  $\tilde{\kappa}_1 \approx 4g^2/\kappa_1$ ,  $\tilde{\kappa}_2 \approx 4g^2\kappa_2/\kappa_1^2$ , and  $\tilde{\kappa}_m \approx g^2\kappa_m/G^2$ . In Fig. 4, we show the fidelity as a function of the system temperature and the decay rate of the optical cavity. It is found that the fidelity is around 99% under typical values of the experimental parameters as listed in the figure caption.

Typically the SQ system is operated around 20 mK temperature, where the ground state cooling is achieved directly through thermal equilibrium. However, with an opto-mechanical interface, the system temperature may increase due to heating by the black-body radiation from the optical window. Here, we show that even under 1 K temperature,

the state can still be initialized through the opto-mechanical sideband cooling. Another requirement for the system temperature is that the quasi-particle density in the superconducting circuit should be small, otherwise it will induce dissipation of the SQ. The quasi-particle density is proportional to  $e^{-1.76T_c/T}$ , where  $T_c$  is the critical temperature of the superconductor [46]. For niobium, the critical temperature  $T_c$  is about 9.3 K, for which the quasi-particle density is negligible at 1 K temperature. For aluminum, the  $T_c$  is about 1.2 K, where the quasi-particles can be neglected only at temperature in the order of 0.1 K.

In summary, we have proposed a scheme to realize a quantum network of SQs base on the opto-mechanical quantum interface. The interface can couple the SQs to optical photons with widely tunable carrier frequencies and pulse shapes. The same interface can also be used for fast initialization of the SQs at 1 K temperature through opto-mechanical sideband cooling.

This work was funded by the NBRPC (973 Program) 2011CBA00300 (2011CBA00302), NNSFC 11105136, 11474177, 61435007. WLY. was supported by the National Fundamental Research Program of China under Grant No. 2012CB922102 and by the NNSFC 11274351. LMD acknowledges support from the IARPA MUSIQ program, the ARO and the AFOSR MURI program.

### Appendix A: Effective linear Hamiltonian

The Hamiltonian of the system takes the form  $H = H_0 + H_I + H_{drive}$ , where

$$H_0 = \sum_{i=1,2} \omega_i a_i^\dagger a_i + \omega_m a_m^\dagger a_m + \omega_e \sigma_{ee},$$

$$H_I = \sum_{i=1,2} g_i a_i^\dagger a_i (a_m + a_m^\dagger) + g_c (\sigma_{eg} + \sigma_{ge}) (a_2 + a_2^\dagger),$$

and

$$H_d = \sum_{i=1,2} \left( \frac{\Omega_i}{2} e^{-i\omega_{L_i} t} + \text{h.c.} \right) (a_i + a_i^\dagger) + \left( \frac{\Omega'}{2} e^{-i\omega_{L_2} t} + \text{h.c.} \right) (\sigma_{ge} + \sigma_{eg}).$$

The SQ is assumed to couple resonantly with the SR with  $\omega_2 = \omega_e$ . The detuning  $\Delta_i = \omega_i - \omega_{L_i} = \omega_m$ . Under the condition that  $\Omega_i < 4\omega_i$ , the Hamiltonian  $H_d$  can be approximated as

$$H'_d = \sum_{i=1,2} \left( \frac{\Omega_i}{2} a_i e^{-i\omega_{L_i} t} + \text{h.c.} \right) + \left( \frac{\Omega'}{2} e^{-i\omega_{L_2} t} + \text{h.c.} \right) (\sigma_{ge} + \sigma_{eg}).$$

We take the rotating wave frame that  $H'_0 = H_0 - \omega_m (a_1^\dagger a_1 + a_2^\dagger a_2)$ . The Hamiltonian in rotating wave frame reads

$$H_R = \omega_m \sum_{p=1,2,m} a_p^\dagger a_p + \sum_{i=1,2} [g_i a_i^\dagger a_i (a_m + a_m^\dagger) + \left( \frac{\Omega_i}{2} a_i + \text{h.c.} \right)] + \omega_e \sigma_{ee} + (g_c a_2 e^{-i\omega_{L_2} t} + \frac{\Omega'}{2} e^{-i\omega_{L_2} t} + \text{h.c.}) (\sigma_{ge} + \sigma_{eg}) \quad (\text{A1})$$

We assume that the decay rates  $\kappa_i$  for mode  $a_i$  ( $i=1,2$ ) are much less than the driving detuning  $\Delta = \omega_m$ . Under the driving, the steady state amplitude of the mode  $a_i$  is given by  $\alpha_i \approx \Omega_i / 2\omega_m$ . In order to compensate the effect of classical driving on SQ, we set  $\Omega'^* = 2\alpha_2 g_c = \Omega_2 g_c / \omega_m$ . In the limit that  $\alpha_i \gg 1$ , the Hamiltonian Eq. (A1) can be expanded with  $a_i - \alpha_i$

$$H_{om} = \sum_{i=1,2} \left[ \omega_m a_i^\dagger a_i + G_i (a_i^\dagger + a_i) (a_m + a_m^\dagger) \right] + \omega_e \sigma_{ee} + \omega_m a_m^\dagger a_m + (g_c a_2 e^{-i\omega_{L_2} t} + \text{h.c.}) (\sigma_{eg} + \sigma_{ge}). \quad (\text{A2})$$

Under the rotating wave approximation ( $\omega_m \gg G_i, g_c$ ), the whole Hamiltonian in the interaction picture is given by

$$H_I = (G_1 a_1^\dagger + G_2 a_2^\dagger) a_m + g_c \sigma_{eg} a_2 + \text{h.c.} \quad (\text{A3})$$

Here we take the parameters we used in Fig. 4 as an example to make sure that the rotating wave approximation is valid. In experiments, the typical parameters are as follows:  $\omega_1/2\pi = 200$  THz,  $\omega_2/2\pi = 10$  GHz, and  $\omega_m/2\pi = 10$  MHz [24, 25, 42],  $\kappa_1/2\pi = 10$  MHz,  $\kappa_2/2\pi = 1$  kHz,  $\kappa_m/2\pi = 10$  Hz,  $\gamma/2\pi = 5$  kHz [44, 45],  $g/2\pi = 1$  kHz, and  $g_c/2\pi = 1$  MHz. The microwave driving strengths are assumed to be  $\Omega = 20$  GHz. The steady state amplitude  $\alpha = 1000$  and  $\Omega' = \Omega * g_c / \omega_m = 2$  GHz. The effective coupling between  $a_2$  and  $a_m$  is  $G_2 = \alpha_2 g_2 = 1$  MHz. With proper driving on optical cavity mode  $a_1$ , we can also get the effective coupling strength  $G_1 = 1$  MHz. Therefore rotating wave approximation condition  $\omega_m \gg G_i, g_2$  is fulfilled.

### Appendix B: Effective Langevin Equation for SQ.

In order to derive the effective Langevin Equation for the SQ, we write down the Langevin equations of the systems

$$\dot{a}_1 = -iG a_m - \frac{\kappa_1}{2} a_1 + \sqrt{\kappa_1} a_1^{\text{in}} \quad (\text{B1})$$

$$\dot{a}_2 = -iG a_m + ig \sigma_{ge} - \frac{\kappa_2}{2} a_2 + \sqrt{\kappa_2} a_2^{\text{in}} \quad (\text{B2})$$

$$\dot{a}_m = -iG (a_1 + a_2) - \frac{\gamma_m}{2} a_m + \sqrt{\kappa_m} a_m^{\text{in}} \quad (\text{B3})$$

$$\dot{\sigma}_{ge} = ig \sigma_z a_2 - \frac{\gamma}{2} \sigma_{ge} + \sqrt{\gamma} \sigma_z \sigma_{ge}^{\text{in}} \quad (\text{B4})$$

In the limit that  $G \gg g, \kappa_1, \kappa_2, \kappa_m$ , we can adiabatically eliminate  $a_m$  and  $a_{1,2}$  modes. Let's solve  $a_m$  from Eq. (B1) in term of  $a_1$ ,

$$a_m = \frac{1}{iG} \left( -\frac{\kappa_1}{2} a_1 + \sqrt{\kappa_1} a_1^{\text{in}} \right), \quad (\text{B5})$$

Then we can solve the  $a_2$  from Eq. (B2) in term of  $a_1$

$$a_2 = \frac{\kappa_1}{\kappa_2} a_1 - \frac{2}{\kappa_2} \sqrt{\kappa_1} a_1^{\text{in}} + \frac{2ig \sigma_{ge}}{\kappa_2} + \frac{2}{\sqrt{\kappa_2}} a_2^{\text{in}}.$$

Let's solve  $a_1$  from Eq. (B3) and get the expression of  $a_2$ ,

$$a_1 = \frac{1}{i \left( G + \frac{\gamma_m \kappa_1}{4G} \right)} \left( -iG a_2 + \frac{i\gamma_m}{2G} \sqrt{\kappa_1} a_1^{\text{in}} + \sqrt{\gamma_m} a_m^{\text{in}} \right).$$

Inserting  $a_1$  into the expression of  $a_2$ , we get that

$$a_2 = \frac{-8G^2 \sqrt{\kappa_1}}{\kappa_2(4G^2 + \kappa_m \kappa_1)} a_1^{\text{in}} - \frac{4iG\kappa_1 \sqrt{\kappa_m}}{\kappa_2(4G^2 + \kappa_m \kappa_1)} a_m^{\text{in}} + \frac{2ig\sigma_{ge}}{\kappa_2} + \frac{2}{\sqrt{\kappa_2}} a_2^{\text{in}} \quad (\text{B6})$$

We get that

$$a_2 = \frac{1}{4G^2(\kappa_1 + \kappa_2) + \gamma_m \kappa_1 \kappa_2} [-8G^2 \sqrt{\kappa_1} a_1^{\text{in}} - 4iG\kappa_1 \sqrt{\kappa_m} a_m^{\text{in}} + (8G^2 + 2\kappa_m \kappa_1) \sqrt{\kappa_2} a_2^{\text{in}} + i(8G^2 + 2\kappa_m \kappa_1) g \sigma_{ge}] \quad (\text{B7})$$

Finally we get the effective Langevin equation for  $\sigma_{ge}$  is

$$\dot{\sigma}_{ge} = - \left( \frac{2g^2 + g^2 \kappa_m \kappa_1 / 2G^2}{(\kappa_1 + \kappa_2) + \kappa_m \kappa_1 \kappa_2 / 4G^2} + \frac{\gamma}{2} \right) \sigma_{ge} + \frac{-2ig \sqrt{\kappa_1} \sigma_z}{(\kappa_1 + \kappa_2) + \kappa_m \kappa_1 \kappa_2 / 4G^2} a_1^{\text{in}} + \frac{i(2 + \kappa_m \kappa_1 / 2G^2) g \sqrt{\kappa_2} \sigma_z}{(\kappa_1 + \kappa_2) + \kappa_m \kappa_1 \kappa_2 / 4G^2} a_2^{\text{in}} + \frac{g\kappa_1 \sqrt{\kappa_m} / G}{(\kappa_1 + \kappa_2) + \kappa_m \kappa_1 \kappa_2 / 4G^2} \sigma_z a_m^{\text{in}} + \sqrt{\gamma} \sigma_z \sigma_{ge}^{\text{in}} \quad (\text{B8})$$

It is easy to verify that the effective Langevin equation (B8) fulfills the Einstein relation.

The effective Langevin equation (B8) for  $\sigma_{ge}$  can be rewritten as

$$\dot{\sigma}_{ge} = -\frac{\gamma_{\text{eff}}}{2} \sigma_{ge} + \sqrt{\gamma_{\text{eff}}} \sigma_z a_{\text{eff}}^{\text{in}}, \quad (\text{B9})$$

where  $\gamma_{\text{eff}}$  and  $a_{\text{eff}}^{\text{in}}$  are defined as

$$\gamma_{\text{eff}} = \gamma + \frac{16G^2 g^2 + 4g^2 \kappa_m \kappa_1^2}{4G^2(\kappa_1 + \kappa_2) + \kappa_m \kappa_1 \kappa_2},$$

and

$$a_{\text{eff}}^{\text{in}} = \left[ \frac{-2ig \sqrt{\kappa_1}}{(\kappa_1 + \kappa_2) + \kappa_m \kappa_1 \kappa_2 / 4G^2} a_1^{\text{in}} + \frac{i(2 + \kappa_m \kappa_1 / 2G^2) g \sqrt{\kappa_2}}{(\kappa_1 + \kappa_2) + \kappa_m \kappa_1 \kappa_2 / 4G^2} a_2^{\text{in}} + \frac{g\kappa_1 \sqrt{\kappa_m} / G}{(\kappa_1 + \kappa_2) + \kappa_m \kappa_1 \kappa_2 / 4G^2} a_m^{\text{in}} + \sqrt{\gamma} a_2^{\text{in}} \right] / \sqrt{\gamma_{\text{eff}}}. \quad (\text{B10})$$

- 
- [1] M. H. Devoret and R. J. Schoelkopf, *Science* **339**, 1169 (2013).  
[2] A. Wallraff, D. I. Schuster, A. Blais, L. Frunzio, R.-S. Huang, J. Majer, S. Kumar, S. M. Girvin and R. J. Schoelkopf. *Nature (London)* **431**, 162 (2004).  
[3] J. Q. You, F. Nori, *Physics Today*, **58**, 42 (2005).  
[4] R. Barends, and *et al.*, *Nature (London)* **508**, 500 (2014).  
[5] Hanhee Paik, and *et al.*, *Phys. Rev. Lett.* **107**, 240501 (2011).  
[6] J. B. Chang, and *et al.*, *Appl. Phys. Lett.* **103**, 012602 (2013).  
[7] S. Olmschenk, D. N. Matsukevich, P. Maunz, D. Hayes, L.-M Duan, C. Monroe, *Science* **323**, 486 (2009).  
[8] J. R. Schaibley, and *et al.*, *Phys. Rev. Lett.* **110**, 167401 (2013).  
[9] H. Bernien, and *em et al.*, *Nature(London)* **497**, 86 (2013).  
[10] D. Kielpinski and *et al.*, *Phys. Rev. Lett.* **108**, 130504 (2012).  
[11] M. Hafezi and *et al.*, *Phys. Rev. A* **85**, 020302(R) (2012).  
[12] J. Verdú and *et al.*, *Phys. Rev. Lett.* **103**, 043603 (2009).  
[13] C. A. Regal and K. W. Lehnert, *J. Phys.: Conf. Ser.* **264**, 012025 (2011).  
[14] J. M. Taylor and *et al.*, *Phys. Rev. Lett.* **107**, 273601 (2011).  
[15] Y. D. Wang, A. A. Clerk, *Phys. Rev. Lett.* **108**, 153603 (2012).  
[16] L. Tian, *Phys. Rev. Lett.* **108**, 153604 (2012).  
[17] Sh. Barzanjeh and *et al.*, *Phys. Rev. Lett.* **109**, 130503 (2012).  
[18] Zheng-Yuan Xue, Zhang-qi Yin, Yan Chen, Z. D. Wang, Shi-Liang Zhu, arXiv:1301.4139.  
[19] Keye Zhang, Francesco Bariani, Ying Dong, Weiping Zhang, Pierre Meystre, arXiv:1410.0070.  
[20] Keyu Xia, Michael R. Vanner, and Jason Twamley, *Scientific Reports* **4**, 5571 (2014).  
[21] R. W. Andrews, and *et al.*, *Nat. Phys.* **10**, 321 (2014).  
[22] F. R. Ong *et al.*, *Phys. Rev. Lett.* **106**, 167002 (2011).  
[23] A. Dewes *et al.*, *Phys. Rev. Lett.* **108**, 057002 (2012); A. Dewes *et al.*, *Phys. Rev. B* **85**, 140503(R) (2012).  
[24] J. D. Teufel and *et al.*, *Nature (London)* **475**, 359 (2011).  
[25] J. D. Teufel and *et al.*, *Nature (London)* **471**, 204 (2011).  
[26] O. Suchoi, K. Shlomi, L. Ella, E. Buks, arXiv:1408.2331.  
[27] Zhang-qi Yin and Yong-jian Han, *Phys. Rev. A* **79**, 024301 (2009).  
[28] Zhang-qi Yin, Fu-li Li, *Phys. Rev. A* **75**, 012324 (2007); Zhang-qi Yin, Fu-li Li, Peng Peng, *Phys. Rev. A* **76**, 062311 (2007).  
[29] I. Wilson-Rae, N. Nooshi, W. Zwerger, and T. J. Kippenberg, *Phys. Rev. Lett.* **99**, 093901 (2007).  
[30] F. Marquardt, J. P. Chen, A. A. Clerk, and S. M. Girvin, *Phys. Rev. Lett.* **99**, 093902 (2007).  
[31] Zhang-qi Yin, *Phys. Rev. A* **80**, 033821 (2009).  
[32] Zhang-qi Yin, Tongcang Li, M. Feng, *Phys. Rev. A* **83**, 013816 (2011).  
[33] Yong-Chun Liu *et al.*, *Chinese Phys. B* **22**, 114213 (2013).  
[34] L. M. Duan, A. Kuzmich, and H. J. Kimble, *Phys. Rev. A* **67**, 032305 (2003).  
[35] J. I. Cirac, P. Zoller, H. J. Kimble, and H. Mabuchi, *Phys. Rev. Lett.* **78**, 3221 (1997).  
[36] Sean D. Barrett and Pieter Kok, *Phys. Rev. A* **71**, 060310(R) (2005).  
[37] Christophe Galland and *et al.*, *Phys. Rev. Lett.* **112**, 143602 (2014).  
[38] C. W. Chou and *et al.*, *Nature (London)* **438**, 828 (2005).  
[39] L. M. Duan, M. Lukin, J. I. Cirac, and P. Zoller, *Nature (London)* **414**, 413 (2001).  
[40] L.-M. Duan and C. Monroe, *Rev. Mod. Phys.* **82**, 1209 (2010).  
[41] W. B. Gao, P. Fallahi, E. Togan, J. Miguel-Sanchez, and A. Imamoglu, *Nature (London)* **491**, 426 (2012).  
[42] J.-M. Pirkkalainen, and *et al.*, *Nature (London)* **494**, 211 (2013).  
[43] T. A. Palomaki, *et al.*, *Nature (London)* **495**, 210 (2013).  
[44] Chad Rigetti and *et al.*, *Phys. Rev. B* **86**, 100506(R) (2012).  
[45] M. Reager, and *et al.*, *Appl. Phys. Lett.* **102**, 192604 (2013).  
[46] J. Bardeen, L. N. Cooper, and J. R. Schrieffer, *Phys. Rev.* **106**,

162 (1957).